A Scalable Spatial Anisotropic Interpolation Approach for Object Removal from Images Using Elastic Net Regularization

M. Raghava(✉), Arun Agarwal, and C. Raghavendra Rao

School of Computer and Information Science,
University of Hyderabad, Hyderabad 500046, India
raghava.m@cvr.ac.in, {aruncs,crrcs}@uohyd.ernet.in

Abstract. Object removal from an image is a novel problem with a lot of applications, in the area of computer vision. The ill-posed nature of the problem and the non-stationary content present in the image render it a complicated task. The diffusion-based and self-similarity based algorithms available in the literature explicitly model either the structures or the textures but not the both. They are good at solving small instances of the problem. However, they tend to produce low fidelity results and turn out to be intractable if the relative size of the object to the input image increases. The moving average based Spatial Anisotropic Interpolation (SAI) for text removal, proposed in our previous work also failed due to its poor extrapolation capability. Thus, it is imperative to develop a sampling scheme which can retain the interpolation feature while showing an apposite concern to the non-stationary features present in the image. The proposed, Design of Computer Experiments (DACE) driven Scalable SAI (SSAI) is a natural extension of SAI in three aspects. Precisely, it extends the Systematic Sampling to 'Not only Symmetric Hierarchical Sampling' (NoSHS), intelligently selects a basis based on Hurst Exponent, and employs Elastic Net regularization of Gaussian regression error for determining the order of the polynomial. Hence, these adaptive features increase the fidelity of the results. This paper elaborates the proposed framework- SSAI and demonstrates its capabilities by comparing the results with the latest hybrid approaches using the PSNR metric.

Keywords: Spatial anisotropic interpolation · DACE · Kriging · Hurst exponent · Elastic net regularization · NoSHS

1 Introduction

In real world situations, an expert artist renovates the damaged wall paintings, manually either by continuing the surrounding information or copying the coherent portions that are present in the vicinity of the target region. Translation of this natural art form into a computer program to process the digital images is a challenge for computer vision community. Researchers from various domains- computational fluid dynamics, mathematics, computer graphics

C. Sombattheera et al. (Eds.): MIWAI 2016, LNAI 10053, pp. 126–140, 2016.
DOI: 10.1007/978-3-319-49397-8_11

and signal processing have been attempting to solve this problem by utilizing the domain-specific tools. The process of restoring the missing portions of an image by using the information available in the neighboring locations, therein the modifications are indiscernible to new observers is called Image Inpainting [1]. The scale of the problem ranges from removal of small scratches to larger objects from images. Let F be the image which is mathematically defined as $F : \Re^m \rightarrow \Re^n$ where $m = 2$ and $n = 3$ for color images; denoting the radiometric color channels Red(R), Green(G) and Blue(B) within RGB model or $n = 1$ for grayscale images. Concerning image inpainting, the input image is assumed to suffer from some degradation process, denoted with an operator T leading to missing of some pixel values. The resulting image I is seen as a composition of two disjoint parts: Ω- represents the locations x at which the pixel values are not known and Φ- corresponds to the locations of which pixel values are known. Ω is considered as the inpaint region and Φ as the source region. Mathematically the degraded/damaged image is expressed as $I = TF$, which is a composition of T and F. The goal of inpainting is to recover the image by estimating the pixel value p_x at all locations $x \in \Omega$ by utilizing the information available in Φ. Hence this problem can be viewed as an inverse problem for which more than one solution may be possible. In literature, such problems are referred to as ill-posed problems [2], and none of the possible solutions is perfect. Object removal is one of the inpainting category problems wherein the region to be filled is large and is of arbitrary shape that renders the task complicated. Figure 1(a) presents an instance of the object removal wherein the man standing to the right is treated as an unwanted object, and the effect of his removal is presented in Fig. 1(b). Overall, an object removal problem is abstracted to ensure that the inpainting model should produce a visually plausible result and retains the overall unity of the image. Now the existing models in the literature are presented briefly.

(a) (b)

Fig. 1. (a) Image with unwanted man present (b) and unwanted man removed

1.1 Local and Greedy Approaches

The first set of formal models for inpainting is derived from Partial Differential Equations (PDE). These methods just fill the missing parts of the image by propagating the information available in the surrounding regions, thereby fall under the local category. Bertalmio [1] pioneered in this field by developing a

non-linear PDE of order three, for controlled transportation of data into the inpaint region, which is named as anisotropic diffusion. Cahn-Hillard equations which are of order four [2] are developed that are capable of interpreting the geometrical structures succinctly. But these methods are less preferred for interactive applications because of their high computational complexity and are best suited for extending small structures only. Another set of models represent the inpaint problem in a variational framework which models the problem as an energy function, and the solutions to minimize it turn out to be ill-posed as the inverse of the energy function is unbounded. A standard way to handle the ill-posed nature is to include some *aprior* information into the model along with the fidelity term, which is referred to as regularization in the literature [2]. The chronological developments in variational models [2] range from simple Total Variation (TV) to Curvature Driven Diffusion (CDD) of information into the inpaint region. These models also come under the local category as they don't involve global features such as large scale textures. The second category of regularization models is based on self-similarity measure which is grossly referred to as exemplar-based methods [3]. These methods iteratively select a patch from the boundary of the inpaint region, analyze its content and search for a similar patch in the source region. Then the best matching patch content is copied into the selected patch. These exemplar-based methods are the examples of non-local methods but work in a greedy manner i.e. they inpaint the hole in a single pass. Though this model seems to be simple, it is necessarily required to answer many design issues that otherwise end up with texture garbages and have a significant bearing on the quality of the result. Even though a lot of variants are derived, the primary features of these methods aim at large-scale texture reproduction but fail to propagate the structures [3].

1.2 Global and Dynamic Approaches

This set of algorithms address the ailments of the local and greedy approaches by defining the inpainting aspect as an *energy* function and evolving an iterative algorithm to minimize it. The energy minimization, for example, is realized by combining multiple patches and verifying the coherence among the neighboring patches. This spatial phenomenon is achieved over a Markov Random Field (MRF) which offers suitable inference algorithms to attain global optimal solutions [4]. The MRF based solutions follow dynamic programming model that strive to achieve spatial coherence [4], among the Exemplar patches while inpainting the image. Authors in [5] observed that the Exemplar patches are separated by the same offset in the image and histogram offer a clue about statistics of dominant offsets. Then the image is shifted based on the dominant offsets, and the resulting images are combined through the MRF framework to achieve better results. But these methods involve manual intervention to separate the texture and structure components and are sensitive to the initial setting.

1.3 Hybrid Approaches

The domain decomposition approaches [6] solve the structure propagation and texture synthesis problems simultaneously by decomposing the image into cartoon and texture components using Morphological Component Analysis (MCA), inpaint both the components independently based on component specific algorithms and combine the partial results to get the overall results. These decomposition based methods are computationally expensive and are capable of filling medium size gaps. Another set of models [7] combine the energy terms related to self-similarity for texture synthesis, diffusion of information for structure Propagation and coherence between inpaint and source region pixels based on the precomputed correspondence map. This method is very sensitive to the initial setting and could solve small scale problems. The latest trend in image inpainting domain is to use non-local statistical information and to combine the Exemplar method with non-local models [8]. These methods are sound in addressing both the functional aspects of inpainting but are applicable for small to medium scale problems. The proposed DACE model attempts to solve the medium to large scale inpainting instance which can address both the texture and structures concurrently without modeling them explicitly.

2 Object Removal as a Spatial Interpolation Problem

For many problems in Computer Vision, it is a formulation necessity to incorporate the notion of representing the gray value or color information of a pixel as a random variable. While imputing the mission values, this association offers a tolerance to a certain degree of variation and is expressed as *error* [9]. The spatial arrangement of random variables $Z(x_i), i = 1 : n$ at locations x_i forms a random field. For example, an image I of size $M \times N$ can represent a random field which is composed of the rectangular arrangement of pixels referring to design sites, and the corresponding pixel values are the responses. In the model building, $X = [x_1, ..., x_m]^T$; $x_i \in \Re^n$ stands for the design sites and $Y = [y_1, ..., y_m]^T$; $y_i \in \Re^q$ represents the corresponding pixel values- the responses. Then an attempt to solve the inpainting problem by casting it as a regular image interpolation problem fails because of its over sensitive nature to the outliers and the absence of error modeling capabilities [9].

2.1 Design and Analysis of Computer Experiments (DACE) Model

DACE [10] is a 'surrogate computer model' which presents the spatial interpolation, namely kriging, in a deterministic way. Kriging model exploits the spatial correlation among the design sites of the underlying random field in contrast to ordinary interpolation which is independent of the location [11]. At a high-level description, kriging model involves the convolution of Polynomial regression with Gaussian regression model. The polynomial regression effectively captures the global patterns (also called as the trend), and the Gaussian regression controls

the prediction error incurred over Ω. Universal kriging [9], a variant of kriging, assumes that the design sites exhibit some trend, and it is possible to capture it, through fitting a higher order polynomial F with unknown coefficients β which constitutes the polynomial regression. Subsequently, kriging controls the prediction error in an unbiased and quantitative manner by associating a stationary field $Z(x)$, which is further governed either by a pre-conceived or well-understood correlation function R. This feature of kriging strikes a behavioral advantage over general regression that analyzes prediction errors through white noise [11]. The combined kriging model could predict the response $\hat{y}$ at a design site x as

$$\hat{y}(x) = \sum_{j=1}^{p} \beta_j F_j + z(x). \tag{1}$$

The first term on the right-hand side in Eq. 1, models the trend through a polynomial regression through an assumed basis F and the unknown coefficients β_j. The second term $z(x)$, $x \in \Re^n$ on the right hand side models the residual over a random field $Z(X)$. The residual is assumed to follow the second order stationary property i.e. the error exhibits zero mean and finite covariance and its minimization requires computation of covariance matrix as $\sigma^2 R(\theta, x_i, x_l)$, for $i, l = 1...m$ where R is the correlation kernel with θ as the parameter and σ is the standard deviation. R, inherently offers a quantitative description for the spatial anisotropy. Thus, kriging addresses the modeling of the given trend and the associated correlation structure simultaneously [13] for computing β. The kriging, as a linear regression model, collects the responses Y at the given design sites in $2 - D$ and predicts the response at an unobserved site x as

$$\hat{y}(x) = C^T Y \quad \text{with} \quad C \in \Re^m. \tag{2}$$

Subsequently, kriging computes three terms: $F = \{F(x_1)...F(x_m)\}^T$- the collocation matrix over the selected basis function, $R = \{R(x_i, x_l)\}$- the spatial correlation expressed in terms of the lag between every pair of design sites i, l and $r(x) = [R(x, x_1), ...R(x, x_m)]^T$- the correlation between every design site x_i and an untried location x. Then the Best Linear Unbiased Estimator (BLUE) of kriging predicts the response at x from Eq. 2 as [10]

$$\hat{y}(x) = r^T R^{-1} Y - \left(F^T R^{-1} r - f\right)^T \left(F^T R^{-1} F\right)^{-1} F^T R^{-1} Y. \tag{3}$$

Now the Generalized Least Square Solution (GLS) for the multivariate polynomial regression [10]

$$F\beta = Y \tag{4}$$

is expressed as

$$\hat{\beta} = \left(F^T R^{-1} F\right)^{-1} F^T R^{-1} Y. \tag{5}$$

The overall predictor can be modeled [10] from Eqs. 3 and 5 as

$$\hat{y}(x) = F^T \hat{\beta} + r^T R^{-1} \quad (Y - F\hat{\beta}), \tag{6}$$

with an estimate of error variance

$$\sigma^2(x) = \frac{1}{m}(Y - F\hat{\beta})^T R^{-1}(Y - F\hat{\beta}). \tag{7}$$

The correlation kernel, in case of 2-D exponential model, is defined as the tensor product of the individual correlations along the columns and the rows

$$R(x, y) = \prod_{p=1}^{2} \exp^{(-\theta_p |d_p|)}. \tag{8}$$

It is evident from the correlation kernel, given in Eq. 8, the correlation decreases exponentially with lag d_p, and the parameter θ_p plays a role in model fitting. In DACE, the parameter θ_p is learned through Maximum Likelihood (ML) principle [10]. Hence, the vector θ can induce the anisotropy if the correlation among the pixel locations along columns differs from the rows.

2.2 Not only Symmetric Hierarchical Sampling Scheme

If the number of design sites grow high then the Kriging model, which involves computation of the inverse for a large scale correlation matrix, suffers from memory hungry problem. This aspect is referred to as 'curse of dimensionality' in the literature [14]. Hence, it is essential to select a subset of representatives from the entire set of available design sites. The proposed Not only Symmetric Hierarchical Sampling scheme (NoSHS) is an extension of the sampling schemes widely used in the super resolution analysis [13]. Systematic Sampling addressed in [14] generates only one sub-image from the input image. Where as, NoSHS produces multiple sub-images recursively by probing the entire image with a dummy element of size $l \times k$ for $l, k \in \{2, 3\}$ and arranges each pixel spanned by the probing element spatially along the rows and the columns of the respective sub-image indexed by l and k. For example, if an image I of size $M \times N$ is subjected to NoSHS for once, with $l = 3$ and $k = 2$ using the Algorithm Extract_6, then the sampling by factor 3 along the row and 2 along the column produces six sub-images I_n with $n = 1 : 6$, each of size $\frac{M}{3} \times \frac{N}{2}$. This sampling stands for an asymmetric instance of NoSHS and is chosen if the underlying image exhibits more spatial correlation along the rows than the columns. In contrast, if the data present in the image exhibits isotropic correlation then Extract_4 (which is not presented in this article) employs a probing element of size is 2×2 and the NoSHS generates four sub-images through symmetric sampling along both the dimensions. Figure 2 presents the functionality of NoSHS which takes a synthetic input image of size 4×4 (column 1) as input and produces 4 sub-images I_1 - I_4 (columns 2–4) of size 2×2. On the input image NoSHS is performed recursively until the size of the Ω present in a sub-image reduces to a minimum. This hierarchical sampling honors the underlying stationary property witnessed in the image and improves the fidelity of prediction process as elaborated in Sect. 2.3. The intuition behind introducing the NoSHS is depicted in the Fig. 3.

$$\mathrm{I} = \begin{matrix} \ulcorner \bullet \circ \bullet \circ \urcorner \\ \diamond \star \diamond \star \\ \bullet \circ \bullet \circ \\ \llcorner \diamond \star \diamond \star \lrcorner \end{matrix} \quad \mathrm{I}_1 = \begin{matrix} \ulcorner \bullet \bullet \urcorner \\ \llcorner \bullet \bullet \lrcorner \end{matrix} \quad I_2 = \begin{matrix} \ulcorner \circ \circ \urcorner \\ \llcorner \circ \circ \lrcorner \end{matrix} \quad I_3 = \begin{matrix} \ulcorner \diamond \diamond \urcorner \\ \llcorner \diamond \diamond \lrcorner \end{matrix} \quad I_4 = \begin{matrix} \ulcorner \star \star \urcorner \\ \llcorner \star \star \lrcorner \end{matrix}$$

Fig. 2. The first column presents a synthetic input image I and the following columns present the sub-images I_1–I_4 extracted through symmetric version of NoSHS from the input image

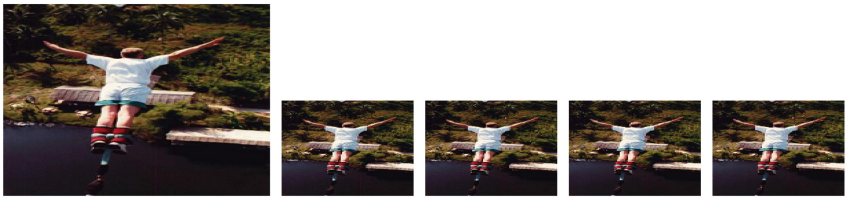

(a) (b) (c) (d) (e)

Fig. 3. (a) Input image [(b)–(e)] The sub-images extracted through NoSHS

Algorithm 1. Extract_6

Input: Input Image I
Output: Extracted Sub-images $I_i; i = 1 : 6$

1. $l := 1;\quad k := 1;; i_2 := 2; j_2 := 2; j_3 := 3;$
2. $for \quad i_1 := 1 : \quad M - 1 :$ `step by 2`
3. $i_2 := i_1 + 1;$
4. $for\ j_1 := 1 \quad : N - 2 :$ `step by 3`
5. $j_2 := j_1 + 1; \quad j_3 := j_1 + 2;$
6. $I_1(l,k) := I(i_1, j_1);$
7. $I_2(l,k) := I(i_1, j_2);$
8. $I_3(l,k) := I(i_1, j_3);$
9. $I_4(l,k) := I(i_2, j_1);$
10. $I_5(l,k) := I(i_2, j_2);$
11. $I_6(l,k) := I(i_2, j_3);$
12. $k := k + 1;$
13. end
14. $l := l + 1; \quad k := 1;; i_2 := i_2 \quad + \quad 2;$
15. end

2.3 Higher Order Polynomial Basis as the Trend

The next criticality of kriging is to solve the multivariate polynomial regression problem which models the trend. The Universal kriging fits a non-linear polynomial basis. However, the nature of the basis and the order of the polynomial are not addressed formally and hence assumes immense importance from

large scale pattern detection point of view. The authors in [15] developed a Bayesian approach based Blind Kriging to resolve this situation. Blind Kriging is essentially the 'multi kriging' model, with a conservative approach involving the fitting of an increasing sequence of orthogonal polynomials, in search of the best-fit polynomial for the input data. Clearly, this approach turns the prediction process a computationally expensive one. The proposed algorithm SSAI addresses the polynomial basis selection issue by employing a futuristic approach which involves kriging, just for once. Initially, for the given design space the correlation R is expressed as the tensor product of the Correlations: one along the rows and the other along the columns, and they may exhibit anisotropy over $Z(X)$. Subsequently, a higher order polynomial F including the cross product terms is selected to model the global trend. For example, if a polynomial basis of order n is selected then the total number of quotients β_k to be learned is $\frac{n(n+1)}{2}$. As the object removal problem entails with a wide range of design sites when compared to the number of candidate terms of higher order polynomial, the chances of wiggling of the regression due to an overfit is less likely. The regression model given in Eq. 5, is a GLS solution that employs the Mahalanobis distance [9] which is scale invariant. This point substantiates that extraction of sub-images from the input image through the NoSHS will not negatively influence the model fitting. Subsequently, the GLS is appropriately regularized with an intention to annihilate the quotients that are either less important or playing spoilsport in predictions. The literature says such a regularization issue is well addressed through feature selection [16], pattern search, etc. The SSAI utilizes the feature selection approach.

2.4 Feature Selection Using Elastic Net

In the proposed model the feature selection is achieved by applying the Elastic net model, developed by Zou and Hastie [16]. Elastic net regularizes the data term with a convex combination of the L_1 (LASSO) and L_2 (ridge) terms of the regression coefficients as

$$\hat{\beta} = \underset{\beta}{\operatorname{argmin}}(\|Y - X\beta\|^2 + \lambda\|\beta\|^2 + (1-\lambda)\|\beta\|_1). \tag{9}$$

It inherently replaces the Euclidean distance measure with checkerboard distance which induces sparsity into the solution and the value of λ determines the level of sparsity. According to the literature [16], small values of λ yields a sparse solution. Thus, even if the trend is modeled with higher order basis, the contribution of particular unnecessary basis terms can be, subsequently curtailed by annihilating the corresponding coefficients to zeros and retaining only the remaining. The future experiments are based on the proposed proactive model and is named as Enhanced DACE (EDACE) which is implemented by utilizing the LARS LASSO [16] model.

3 Adaptive Basis Selection

The object removal algorithm SSAI is capable of selecting a basis from the predefined collection of different basis functions in an adaptive manner. From our empirical observations, the nature of the polynomial can be a constant or any higher order polynomial, each of them with varying capabilities while modeling the trend. The subjective issue of basis selection is addressed by extracting the Hurst exponent H [17]. $H \in [0 \quad 1]$, is a self-similarity based measure capable of manifesting the non-stationary behavior present in the content of the image. Signal process community uses H for measuring the strength of singularity [18]. Hurst exponent describes the probability with which the autocorrelation among the pixels of the image changes asymptotically with the lag h as follows:

$$E[\frac{R(h)}{S(h)}] = Ch^H \qquad as \qquad \mathrm{h} \rightarrow \quad \infty, \tag{10}$$

where R refers to the range of values spanned by h, S represents the standard deviation of the data and C is a constant. H value can be estimated in various ways such as Box Counting, Rescaled Range Analysis [18], Wavelet Spectral Density, etc., and is extended to 2-D images also [15]. To understand Hurst exponent, R/S- one of the estimation methods, is discussed for 1-D data. Given $y_i; \quad i = 1 : n$ the pixel responses at locations $x_i; \quad i = 1 : n$ with mean m, then calculate the deviations d_i of each y_i from m using $d_i = y_i - m$. The series of partial sums p_i over d_i are calculated in a cumulative manner as detailed in Eq. 11.

$$s_k = \sum_{l=1:k} d_l \qquad k = 1 : n. \tag{11}$$

Then the difference of $max\{s_k\}$ and $min\{s_k\}$ denotes Range R and the slope of 'bestfit' line for $\log(\frac{R}{S}) \quad vs \quad \log(n)$ represents the *estimate* of Hurst exponent H. Inherently, it models the Fractal coefficient which is a measure of self-similarity of Brownian motion [17]. The *estimated* Hurst exponent value, can be utilized to characterize the underlying process into three classes: stationary, not-known and non-stationary. The proposed SSAI utilizes the value of H to categorize the images into two classes as follows. If $H \in [0 \quad 0.5]$, then the image is classified to possess second order stationary trend and is modeled by deploying a higher order polynomial. Otherwise, the content of the image is assumed to be smooth, and the trend is represented through a constant. This adaptive feature in SSAI is a novel contribution in inpainting domain and avoids the formulations for texture and structure specific components.

4 The PushBack Operation

As the last step in the proposed framework, all inpainted sub-images belonging to a particular level of the hierarchy required being systematically combined in an anti-recursive manner to get the overall result. It is a PushBack

of the chosen hierarchical sampling that merely rearranges the pixels from each inpainted sub-image back into their proper locations until the original size of the input image is reached. Algorithm $PushBack\_4$ takes the 4 inpainted sub-images $I_i, i = 1:4$, in the case of symmetric sub-sampling by order 2, and reconstructs the original image I. A similar algorithm can be evolved for Asymmetric Push-Back_6 through a relatively simple effort.

Algorithm 2. PushBack_4

Input: Set of all 4 inpainted sub-images $I_i, i = 1:4$ each of size $m \times n$ that are extracted from I
Output: Reconstructed image I

1. $for \quad i := 1:m: \quad step \quad by \quad 1$
2. $for \quad j := 1:n: \quad step \quad by \quad 1$
3. $I(2 \times i - 1, 2 \times j - 1) := I_1(i, j);$
4. $I(2 \times i - 1, 2 \times j) := I_2(i, j);$
5. $I(2 \times i, 2 \times j - 1) := I_3(i, j);$
6. $I(2 \times i, 2 \times j) := I_4(i, j);$
7. end
8. end

5 The Algorithm: SSAI

Algorithm SSAI, summarizes the steps discussed so far and presents the complete algorithm for object removal from images. If the input image possesses the correlation which is same along the rows and columns then their tensor product gains circular shape (see Fig. 4(a)) and the symmetric kernel of the proposed NoSHS, Extract_4 carries out uniform sampling and extracts four sub-images. In contrast to this, if the correlation is more prominent along the columns than the rows then their tensor product assumes elliptic shape, as shown in Fig. 4(b). Then the asymmetric kernel of NoSHS, Extract_6 performs coarse sampling along the columns and fine-grained sampling along the rows to derive 6 sub-images.

Fig. 4. (a) presents the pictorial representation of the Isotropic correlation in which case symmetric kernel for sampling is required and (b) presents the Anisotropic correlation that prompts the selection of asymmetric sampling kernel

Finally, the EDACE model is developed for predicting the pixel values at inpaint locations for each sub-image.

Algorithm 3. SSAI

Data: Input Image I and the associated Mask M
Result: Inpainted image

1. Derive H from I
2. `Select the forward sampling kernel Sect. 2.2 under NoSHS`
3. `Check the size of the inpaint region and determine the levels of hierarchy` k
4. `Apply the chosen NoSHS scheme on` I `and` M `to extract` $\mathbb{k}$ `sub-images`
5. `Select the sub-images available at bottom-most level of the hierarchy and put them into array` A
6. `Choose a basis` F `to represent the trend based on` H `and the correlation model` R.
7. `Fit EDACE model for every sub-image on` A `and predict the responses over` Ω
8. `Invoke the corresponding PushBack kernel Sect. 4 recursively on inpainted sub-images, about step 2, to produce the inpainted image.`

6 Experiments and Results

Experiment 1. The fidelity gain through Elastic net regularization-

Here we demonstrated the effect of the Elastic net regularization term introduced in the proposed model. In this experiment, initially a fifth order polynomial with 21 coefficients was selected to represent the trend in the course of polynomial regression. The over sensitive nature of the linear regression to the outliers was addressed by Elastic net regularization while eliminating the non-essential coefficients of the higher order polynomial. This improved the fidelity of the results as shown in Fig. 5- compare Fig. 5(b) with 5(c) and Fig. 5(e) with 5(f).

Experiment 2. Structure and Texture preserving capabilities without modeling them explicitly-

In Experiment 2, images with a large whole marked in white color were taken up. SSAI modeled the trend as a constant and employed the exponential correlation basis for the input images in Fig. 6(a) and (g). We could observe that SSAI was able to fill the holes, see Fig. 6(b) and (h), with a meaningful content on both sides of the linear structures. The anisotropy feature of the interpolation resolved the confusion as to extend the horizontal structure or vertical structure and achieved the better control. In Fig. 6(c) and (d), the staircase was preserved thoroughly by propagating the information along the structures. The image in Fig. 6(e) possesses small H value and is considered to be non-stationary image

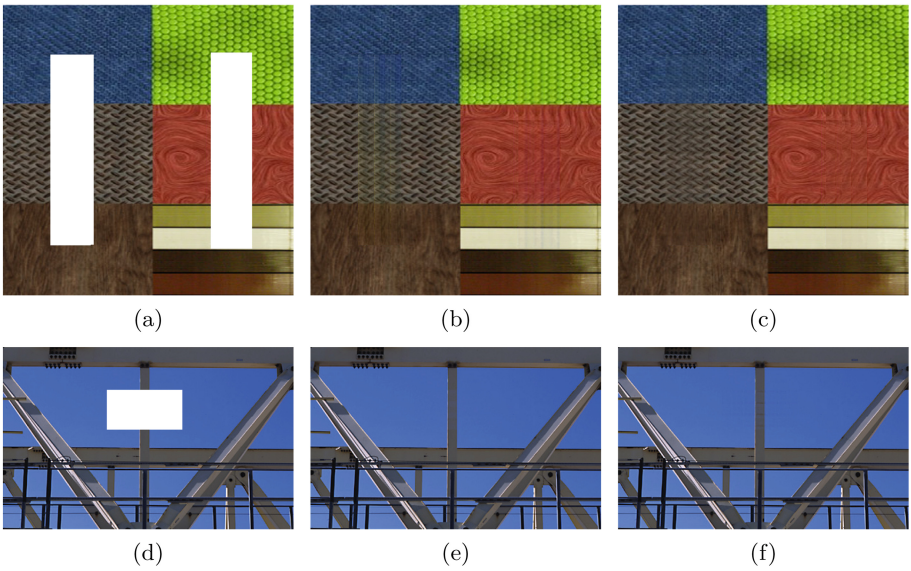

Fig. 5. Column1 presents the input images, column 2 presents the results of the proposed SSAI model and column 3 presents the results in the absence of Elastic net regularization.

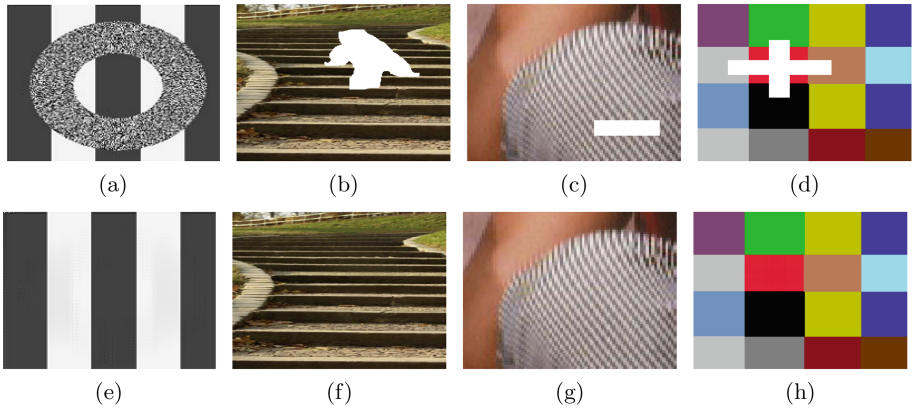

Fig. 6. Row 1 presents the input images. Row 2 presents the corresponding inpainted results of SSAI Model.

and Fig. 6(f) demonstrated the capability of SSAI model to synthesize the fine texture.

Experiment 3. Large Scale object Removal - comparison with Hybrid approach

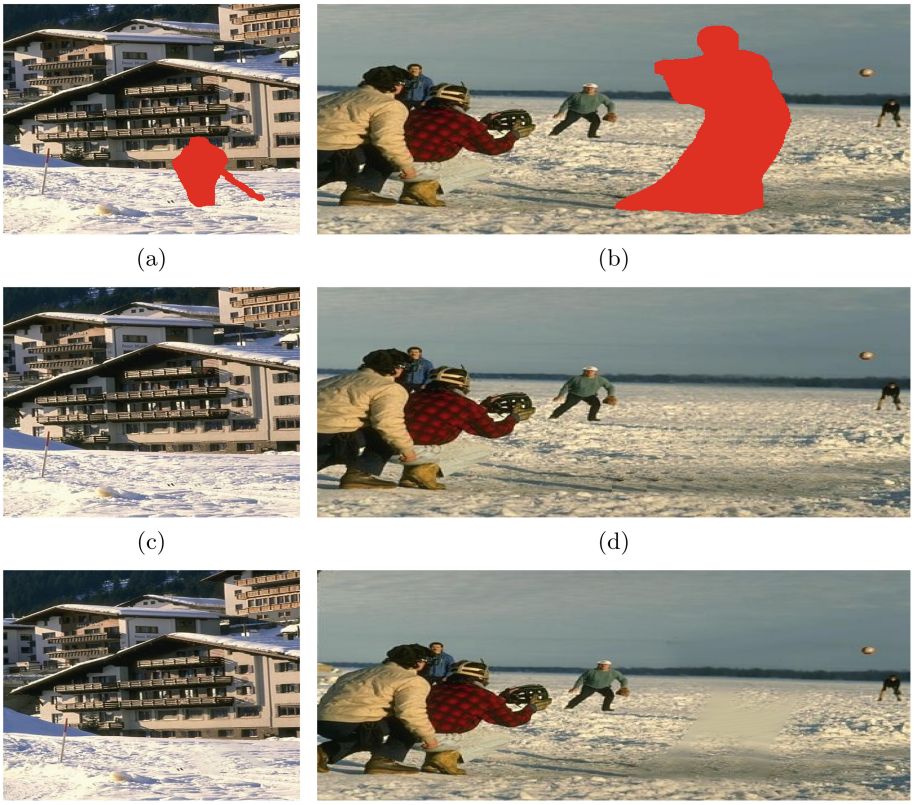

Fig. 7. Row 1- Input images, row 2 presents the results of SSAI and row 3 presents the results of Aria's [7] method.

Table 1. The Hurst exponent based Decision Table and the improvement in PSNR through SSAI

Image	H	Nature	Basis	Before	After
Grid-6(d)	0.89	Stationary	Constant	16.8 db	59.41 db
Trouser-6(c)	0.19	Second-order-stationary	Polynomial	22.6 db	39.76 db
Gantry-5(e)	0.42	Second-order-stationary	Polynomial	16.32 db	46.45 db

In this experiment, Fig. 7, the input images that had cartoon components and texture elements separated by structures were considered. SSAI preserved the structures and interpolated the texture components successfully. Whereas [7], a non-local Total Variational method failed to synthesize the textures clearly, compare Fig. 7(c) with 7(e) and Fig. 7(d) with 7(f). The efficacy of the adaptive basis selection feature of the proposed SSAI model and the quality of results in PSNR values are presented in Table 1.

7 Summary

In this paper, the object removal problem was solved without involving 'locate and copy' or diffusion of information models which were developed around the texture and structure components. In contrast, the proposed SSAI, employed the anisotropy based sampling scheme NoSHS, and addressed the ill-posed nature of the problem, through an adaptive polynomial basis selection based on Hurst exponent. The SSAI enhanced the quality of the solution through Elastic net regularization and overcome the stigma of Blind kriging over DACE. The experiments established the fact that high fidelity results are realizable for large scale inpainting problems through the properly modeled spatial interpolation.

References

1. Bugeau, A., Bertalmio, M., Caselles, V., Sapiro, G.: A comprehensive framework for image inpainting. IEEE Trans. Image Process. **19**(10), 2634–2645 (2010)
2. Guillemot, C., Le Meur, O.: Image inpainting: overview and recent advances. IEEE Signal Process. Mag. **31**, 127–144 (2014)
3. Buyssens, P., David, T., Olivier, L.: Exemplar-based inpainting: technical review and new heuristics for better geometric reconstructions. Trans. IP **24**, 1809–1824 (2015)
4. Komodakis, N., Georgios, T.: Image completion using efficient belief propagation via priority scheduling and dynamic pruning. IEEE Trans. Image Process. **16**, 2649–2661 (2007)
5. He, K., Sun, J.: Statistics of patch offsets for image completion. In: Fitzgibbon, A., Lazebnik, S., Perona, P., Sato, Y., Schmid, C. (eds.) Computer Vision, ECCV 2012. LNCS, vol. 7573, pp. 16–29. Springer, Heidelberg (2012)
6. Elad, M., Starck, J., Querre, P., Donoho, D.L.: Simultaneous cartoon and texture image inpainting using morphological component analysis (MCA). Appl. Comput. Harmon. Anal. **19**, 340–358 (2005)
7. Barnes, C., Shechtman, E., Finkelstein, A., Goldman, D.: Patchmatch: a randomized correspondence algorithm for structural image editing. ACM Trans. Graph. **28**, 24:1–24:11 (2009)
8. Arias, P., Facciolo, G., Caselles, V., Sapiro, G.: A variational framework for exemplar-based image inpainting. Int. J. Comput. Vis. **93**, 319–347 (2011)
9. Cressie, N.: Statistics for Spatial Data, vol. 416. Wiley, Hoboken (1993)
10. Lophaven, N., Nielsen, H.B., Jacob, S.: IMM. Informatics and Mathematical Modeling. Technical University of Denmark, DACE A Matlab Kriging Toolbox (2002)
11. Gentile, M., Courbin, F., Meylan, G.: Interpolating point spread function anisotropy, aap (2013)
12. Miller, A.J.: Subset Selection in Regression. Chapman & Hall, Boca Raton (2002)
13. Miaohui, W., Bo, Y., King, N.: An efficient framework for image, video inpainting. Signal Process.: Image Commun. **28**, 753–762 (2013)
14. Raghava, M., Agarwal, A., Rao, C.R.: Spatial anisotropic interpolation approach for text removal from an image. In: Ramanna, S., Lingras, P., Sombattheera, C., Krishna, A. (eds.) MIWAI 2013. LNCS (LNAI), vol. 8271, pp. 153–164. Springer, Heidelberg (2013). doi:10.1007/978-3-642-44949-9_15
15. Couckuyt, I., Forrester, A., Gorissen, D., De Turck, F., Dhaene, T.: Blind Kriging: implementation and performance analysis. Adv. Eng. Softw. **49**, 1–13 (2012)

16. Zou, H., Hastie, T.: Regularization and variable selection via the elastic net. J. R. Stat. Soc. **67**, 301–320 (2005)
17. Orietta, N., Garutti, C., Vidakovic, B.: 2-D wavelet-based spectra with application in analysis of geophysical images, GIT, February 2006
18. Carbone, A.: Algorithm to estimate the Hurst exponent of high-dimensional fractals. Phys. Rev. E **76** (2007)